Journal of Coastal Research	SI	73	771-775	Coconut Creek, Florida	WINTER 2015

Feed Forward Compensation Control of Dual-Axis Photoelectric Stabilized Platform

Changjing Xie[†*], Zhiqiang Wang[‡], Rui Wang[†], and Zhenhua Jiang[†]

[†]Changchun Institute of Optics
Fine mechanics and Physics
Chinese Academy of Science
Changchun 130033, China

[‡]Beijing University of Aeronautics and Astronautics
Beijing 100191, China

www.cerf-jcr.org

www.JCRonline.org

ABSTRACT

Xie, C.; Wang, Z.; Wang, R., and Jiang, Z., 2015. Feed forward compensation control of dual-axis photoelectric stabilized platform. *In*: Mi, W.; Lee, L.H.; Hirasawa, K., and Li, W. (eds.), *Recent Developments on Port and Ocean Engineering*. Journal of Coastal Research, Special Issue, No. 73, pp. 771-775. Coconut Creek (Florida), ISSN 0749-0208.

The carrier angular motion and disturbance torque are the two main problems limiting stable accuracy of the line of sight (LOS) of airborne optical stabilized platform. Angular rate isolation and torque stiffness analysis of the servo system are proposed to improve the stable accuracy. A PII^2 control scheme is taken to obtain fast response, low overshot and zero steady-state error. In order to achieve higher target tracking precision compared with PII^2 scheme, a feed forward compensation has been presented against the low tracking accuracy problems caused by pure lag of the system image tracking instruction. Simulation results indicate that the servo system designed has strong capability of isolating angular movement and disturbance torque. Tracking accuracy of the stabilized platform servo control system can be efficiently improved when appropriate feed forward control is introduced.

ADDITIONAL INDEX WORDS: *LOS, photoelectric stabilized platform, torque stiffness, PII^2 control, feed forward compensation, pure lag.*

INTRODUCTION

Last few years, airborne optical stabilized platform has been widely used in military operation, law enforcement, border patrol operations and other civilian areas such as monitoring wetland, weather forecasting and surveying hurricane and disaster damage (Klemas, 2014; Qadir, Semke, and Neubert, 2011). The ever increasing prevalence of UAV, combined with the rapid progression of imaging systems and gyro technologies, has facilitated the evolution of high performance, low cost optical stabilized platform (Miller, Mooty, and Hilkert, 2013). Stabilizing and tracking are the main task of the optical stabilized platform. The servo system ensures the LOS timely and accurate target tracking, which makes the stabilization control of the LOS become the important part of the optical tracking system and decide the system tracking precision (Chang, Hou, and Tsai, 2013; Chen Jiao, and Wu, 2012).

Recently, the relevant researches about photoelectric stabilized platform mainly concentrate on two fields. One is PII^2 (proportional-integral-double integral) control, based on angular rate feedback and angular feedback, designed in frequency domain, which has the advantage of zero steady-state error (Han, Lu, and Qiu, 2007). Another is employing modern control algorithm, such as Adaptive Sliding Mode Variable Structure Control and H Infinity / Predictive control (Darestani, Nikkhah, and Sedigh, 2014). Through PII^2 control, system will have fast response and low overshot in angular motion isolation. Besides, PII^2 control can achieve zero steady-state error of angular output because of its double integrals. However, PII^2 control can not attain fast response and high tracking precision because of the pure lag of system image tracking instruction (Hurak and Rezac, 2010; Zdenek and Martin, 2012). Through Adaptive Sliding Mode Variable Structure Control or H Infinity / Predictive control, the robustness and adaptability of system have been improved in the face of the model parameter variations and unknown disturbances (Chang, Chuang, and Tsai, 2012; Chang, Hou, and Tsai, 2013). These researches are usually based on robust and optimal theory, and they improve the dynamic response more successfully than steady-state performance. These kinds of control scheme generally cannot obtain zero steady-state error, which is an extremely significant indicator in stabilized platform.

In this paper, the author analyses the stabilized principle when both azimuth gyro and elevation gyro are mounted in elevation frame, which are the most efficient installation compared with other indirect approaches of gyro mounting (Hilkert and Amil, 2010; Kennedy and Kennedy, 2003). Another important part is the motor servo system. To achieve zero steady-state error, PII^2 control scheme has been analyzed and employed in this servo system. And a feed forward compensation has been introduced to increase the response rate against the pure lag in target tracking.

Stabilized algorithm, including choosing gyros' installation location, is the first thing that needs to be considered in an optical stabilized platform (Hilkert, 2008). Schematic of dual-axis gyro stabilized platform is presented in Figure 1. The platform is composed by azimuth frame and elevation frame. $oX_dY_dZ_d$: base coordinate; $oX_aY_aZ_a$: azimuth frame coordinate;

DOI: 10.2112/SI73-132.1 received 21 August 2014; accepted in revision 16 November 2014.

*Corresponding *author*: xiechangjing@163.com

$oX_fY_fZ_f$: elevation frame coordinate; θ_a , θ_f : azimuth angular, elevation angular.

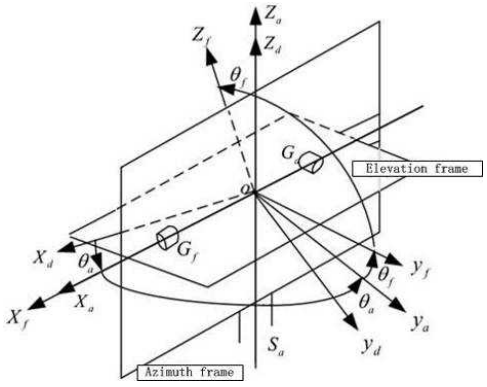

Figure 1. Schematic of dual-axis gyro stabilized platform.

THEORY OF ANGULAR MOTION ISOLATION

The coordinate transformation between the base coordinate frame and azimuth coordinate frame is (note: a "bar" denotes a matrix, and a "hat" denotes a vector)

$$\overline{C}_d^a = \begin{bmatrix} c_{\theta_a} & s_{\theta_a} & 0 \\ -s_{\theta_a} & c_{\theta_a} & 0 \\ 0 & 0 & 1 \end{bmatrix}; c_{\theta_a} = \cos(\theta_a); s_{\theta_a} = \sin(\theta_a)$$

The base coordinate frame rate vector $\hat{\omega}_{id}^d(t)$ is related to the outer coordinate frame rate vector $\hat{\omega}_{ia}^a(t)$ by

$$\hat{\omega}_{ia}^a(t) = \overline{C}_d^a * \hat{\omega}_{id}^d(t) + \hat{\dot{\theta}}_a(t) \quad (1)$$

Where

$$\hat{\omega}_{id}^d(t)^T = [\omega_{idx}^d \quad \omega_{idy}^d \quad \omega_{idz}^d], \hat{\dot{\theta}}_a(t)^T = [0 \quad 0 \quad \dot{\theta}_a]$$

The coordinate transformation between the azimuth frame and elevation frame is given by

$$\overline{C}_a^f = \begin{bmatrix} 1 & 0 & 0 \\ 0 & c_{\theta_f} & s_{\theta_f} \\ 0 & -s_{\theta_f} & c_{\theta_f} \end{bmatrix}; c_{\theta_f} = \cos(\theta_f); s_{\theta_f} = \sin(\theta_f)$$

The elevation coordinate frame rate vector $\hat{\omega}_{ia}^a(t)$ is related to the azimuth coordinate frame rate vector $\hat{\omega}_{if}^f(t)$ by

$$\hat{\omega}_{if}^f(t) = \overline{C}_a^f * \hat{\omega}_{ia}^a(t) + \hat{\dot{\theta}}_f(t) \quad (2)$$

Where

$$\hat{\dot{\theta}}_f(t)^T = [\dot{\theta}_f \quad 0 \quad 0], \quad \hat{\omega}_{if}^f(t)^T = [\omega_{ifx}^f \quad \omega_{ify}^f \quad \omega_{ifz}^f]$$

We can infer from Equation (1) and Equation (2) that

$$\hat{\omega}_{if}^f(t) = \overline{C}_a^f * \overline{C}_d^a * \hat{\omega}_{id}^d(t) + \overline{C}_a^f * \hat{\dot{\theta}}_a(t) + \hat{\dot{\theta}}_f(t) \quad (3)$$

In detail

$$\begin{bmatrix} \omega_{ifx}^f \\ \omega_{ifz}^f \end{bmatrix} = \begin{bmatrix} 1 & 0 \\ 0 & c_{\theta_f} \end{bmatrix} \begin{bmatrix} \dot{\theta}_f \\ \dot{\theta}_a \end{bmatrix} + T_2 \begin{bmatrix} \omega_{idx}^d \\ \omega_{idy}^d \\ \omega_{idz}^d \end{bmatrix} \quad (4)$$

Angular rate coupling matrix:

$$T_2 = \begin{bmatrix} c_{\theta_a} & s_{\theta_a} & 0 \\ s_{\theta_a} * s_{\theta_f} & -c_{\theta_a} * s_{\theta_f} & c_{\theta_f} \end{bmatrix}$$

When both azimuth gyro and elevation gyro are mounted in the elevation frame, angular rate output of the azimuth gyro and elevation gyro can be represented as:

$$\hat{\omega}_p(t)^T = [\omega_{px} \quad \omega_{pz}]$$

Where

$$\begin{bmatrix} \omega_{px} \\ \omega_{pz} \end{bmatrix} = \begin{bmatrix} c_{\theta_a} & s_{\theta_a} & 0 \\ s_{\theta_a} * s_{\theta_f} & -c_{\theta_a} * s_{\theta_f} & c_{\theta_f} \end{bmatrix} \begin{bmatrix} \omega_{idx}^d \\ \omega_{idy}^d \\ \omega_{idz}^d \end{bmatrix} \quad (5)$$

We can conclude from Equation (4) and Equation (5) that

$$\begin{bmatrix} \omega_{px} \\ \omega_{pz} \end{bmatrix} = \begin{bmatrix} 1 & 0 \\ 0 & c_{\theta_f} \end{bmatrix} \begin{bmatrix} \dot{\theta}_f \\ \dot{\theta}_a \end{bmatrix} + \begin{bmatrix} \omega_{px} \\ \omega_{pz} \end{bmatrix} \quad (6)$$

Therefore,

$$\begin{bmatrix} \dot{\theta}_f \\ \dot{\theta}_a \end{bmatrix} = \begin{bmatrix} 1 & 0 \\ 0 & 1/c_{\theta_f} \end{bmatrix} \begin{bmatrix} \omega_{ifx}^f - \omega_{px} \\ \omega_{ifz}^f - \omega_{pz} \end{bmatrix} \quad (7)$$

Equation (7) is the stable algorithm of dual-axis gyro stabilized platform when both azimuth gyro and elevation gyro are installed in the elevation frame.

MOTOR SERVO SYSTEM DESIGN

In order to obtain LOS stabilization of high precision, airborne optoelectronic stabilized platform utilize the motor servo system of multiple closed loops to reduce the deviation of LOS caused by angular motion, vibration, and torque disturbance. In addition, the servo system cannot obtain real time target tracking without achieving fast response velocity. Considering all those requirements, a system of high forward gain, strong dynamic stiffness, and ultra-low response time has been designed. Control structure of angular rate loop (take azimuth loop as an example) is shown in Figure 2.

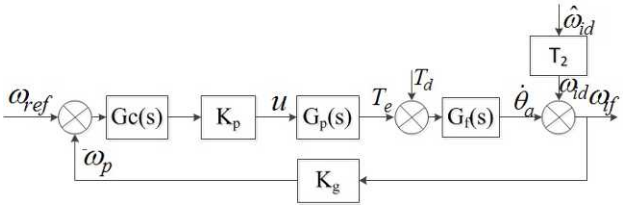

Figure 2. Angular rate stabilizing control loop.

$G_c(s)$: Transfer function of stabilizing controller. K_p : Amplification coefficient of power driver. $G_p(s)$: Transfer function of torque motor. $G_f(s)$: Transfer function of frame components. K_g : Gyro scaling factor. T_2 : Base angular rate coupling matrix.

We can infer from Figure 2 that

$$\omega_{if}(s)=\frac{k_pG_c(s)G_p(s)G_f(s)\omega_{ref}(s)+G_f(s)T_d(s)+\omega_{id}(s)}{1+k_gk_pG_c(s)G_p(s)G_f(s)} \quad (8)$$

Suppose

$$\omega_{if1}(s)=\frac{k_pG_c(s)G_p(s)G_f(s)}{1+k_gk_pG_c(s)G_p(s)G_f(s)}\omega_{ref}(s)$$

$$\omega_{if2}(s)=\frac{G_f(s)}{1+k_gk_pG_c(s)G_p(s)G_f(s)}T_d(s)$$

$$\omega_{if3}(s)=\frac{1}{1+k_gk_pG_c(s)G_p(s)G_f(s)}\omega_{id}(s)$$

Where $\omega_{if1}(s)$ is the desired angular rate output, $\omega_{if2}(s)$ is the deviation angular rate caused by disturbance torque, $\omega_{if3}(s)$ is the deviation angular rate caused by base angular motion.

We have

$$T_s(s)=Js^2+k_gk_psG_c(s)G_p(s) \quad (9)$$

We call $T_s(s)$ as the torque stiffness of the platform. Where J : Load inertia, $\theta_{if2}(s)=\omega_{if2}(s)/s$, $T_s(s)=T_d(s)/\theta_{if2}(s)$, $G_f(s)=1/Js$.

In order to achieve a zero deviation angle, $G_c(s)$ must include an integral part. Suppose $G_c(s)=G_c'(s)/s$. Substitute s with $j\omega$ in Equation (9). We obtain the frequency characteristics of the torque stiffness.

$$T_s(j\omega)=J(j\omega)^2+k_gk_pG_c'(j\omega)G_p(j\omega) \quad 10)$$

We employ lead-lag correction to design angular rate stabilizing controller, which can make sure servo system achieving a high stability margin and an ultra-low response time. Curve of torque stiffness is plotted in Figure 3.

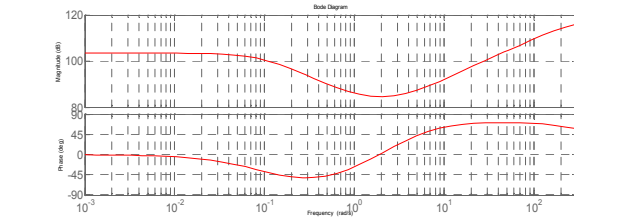

Figure 3. Bode diagram of dynamic torque stiffness.

SIMULATION

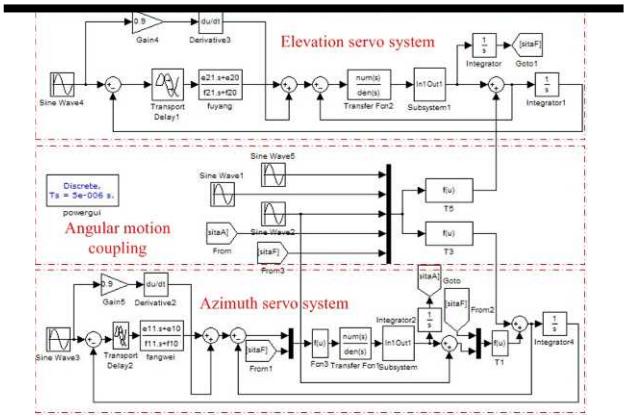

Figure 4. Simulation model.

Utilizing the simulation model in Figure 4, we have the unit step responses of angular rate loops showed in Figure 5.

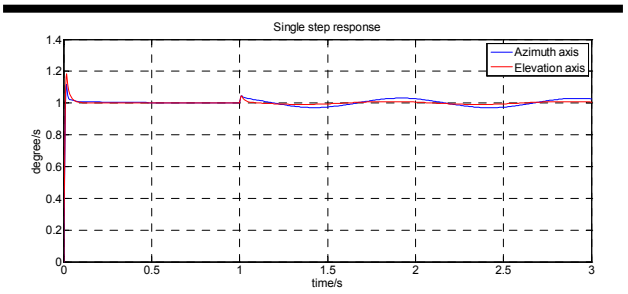

Figure 5. Unite step responses of angular rate loops.

The simulation results tell the system can attain fast response

rate and required stabilized accuracy of angular rate of $0.22209\,rad/s$. Simulation conditions: constant torque disturbance $T_d = 1$ Nm, a friction torque of 0.015 Nm. Note: there is no base angular motion between zero and the first seconds, a base angular motion $\omega_{idx}^d = \omega_{idy}^d = \omega_{idz}^d = 0.0262\sin(2\pi t)\,rad/s$ is injected between the first seconds and the third seconds.

The results of position tracking experiments for azimuth-axis and elevation-axis are shown in Figure 6 and Figure 7. Simulation conditions: azimuth reference input $0.436\cos(0.2\pi t)\,rad$, elevation reference input $0.436\sin(0.2\pi t)\,rad$, pure lag time $t = 10$ ms, constant torque disturbance $T_d = 1$ Nm, a friction torque of 0.015 Nm, base angular motion $\omega_{idx}^d = \omega_{idy}^d = \omega_{idz}^d = 0.0262\sin(2\pi t)\,rad/s$.

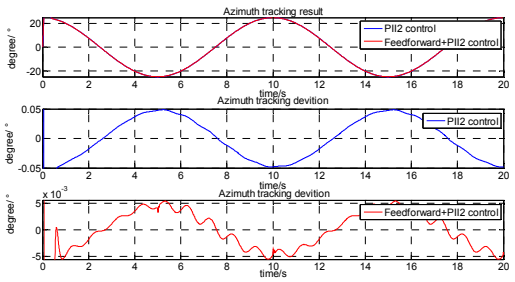

Figure 6. Azimuth tracking result and corresponding tracking deviation.

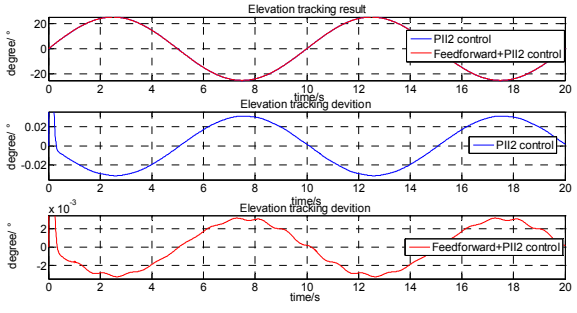

Figure 7. Elevation tracking result and corresponding tracking deviation.

As can be seen from the Figurers, error curve of the PII^2 control is smoother than that of feed forward compensation control, whose error contains more high-frequency component. However, the error precision of the feed forward compensation is much higher than the PII^2 control.

CONCLUSIONS

A position-angular rate PII^2 control system has been established based on the angular motion isolation and torque stiffness analysis of the airborne optical stabilized platform. Feed forward compensation, combined with PII^2 control, can efficiently improve the response rate and target tracking precision. Principle of stabilization has been verified. The simulation results show the correctness and feasibility of the approaches.

ACKNOWLEDGMENTS

This paper is funded by Project of National Natural Science Foundation of China (51107002).

LITERATURE CITED

Chang, Y.Z.; Chuang, S.C., and Tsai, Z. R., 2012. Adaptive Inverse Control of a Temperature Regulation System with Feed forward. *IEEE International Conference on Fuzzy Systems* (Taipei, Taiwan), pp.1026-1032.

Chang, Y.Z.; Hou, J.F., and Tsai, Z.R., 2013. Adaptive Neuro-Like Control of Time-Delay Systems enhanced with Feed forward and Supervisory Strategies. *Mathematical Problems in Engineering*, 25-29.

Chen, W.S.; Jiao, L.C., and Wu, J.S., 2012. Globally stable adaptive robust tracking control using RBF neural networks as feedforward compensators. *Neural Computing & Applications,* 21(2), 351-363.

Darestani, M.R.; Nikkhah, A.A., and Sedigh. A.K., 2014. Hinfinity/Predictive output control of a three axis gyro stabilized platform. *Journal of Aerospace Engineering,* 228(5), 679-689.

Han, Y.G., Lu, Y.H., and Qiu, H.T., 2007. An Improved Control Scheme of Gyro Stabilization Electro-Optical Platform*, IEEE International Conference on Control and Automation* (Jinan, Shandong, China), pp.346-351.

Hilkert, J.M., 2008. Inertially stabilized platform technology: concepts and principles. *Control Systems, IEEE,* 28(1),26–46.

Hilkert, J.M. and Amil, D.L., 2010. Structural effects and techniques in precision pointing and tracking systems-a tutorial overview. *SPIE Proceedings*, 7696, 52-63.

Hurak, Z. and Rezac, M., 2010. Delay compensation in a dual-rate cascade visual servomechanism. *49th IEEE Conference on Decision and Control* (Atlanta, Georgia USA), pp. 1639-1643.

Kennedy, P.J. and Kennedy, R.L., 2003. Direct Versus Indirect Line of Sight (LOS) Stabilization. *IEEE Transactions on Control System Technology*, 11(1), 3-15.

Klemas, V., 2014. Remote Sensing of Riparian and Wetland Buffers: An Overview. *Journal of Coastal Research*, 30(5), 869-880.

Miller, R.; Mooty, G., and Hilkert, J.M., 2013. Gimbal system configurations and line-of-sight control techniques for small UAV applications. *SPIE Proceedings*, 8713, 56-70.

Qadir, A., Semke, W., and Neubert, J., 2011. Implementation of an Onboard Visual Tracking System with Small Unmanned

Aerial Vehicle (UAV). *Innovative Technology & Creative Engineering*, 1 (10), 17-25.

Zdenek, H. and Martin, R., 2012. Image-Based Pointing and Tracking for Inertially Stabilized Airborne Camera Platform. *IEEE Transactions on Control System Technology*, 20(5), 1146-1159.